Application of tensor CSAMT with high-power orthogonal signal sources in Jiama porphyry copper deposit in Tibet

Peng-liang Yu, Ting Qu, Ri-zheng He, Jian-li Liu, Su-fen Wang, Xiao-long Chen

Citation: Peng-liang Yu, Ting Qu, Ri-zheng He, Jian-li Liu, Su-fen Wang, Xiao-long Chen, 2021. Application of tensor CSAMT with high-power orthogonal signal sources in Jiama porphyry copper deposit in Tibet, China Geology, 4, 1-13. doi: 10.31035/cg2021065.

View online: https://doi.org/10.31035/cg2021065

China Geology 4 (2021) 1−13

China Geology

Journal homepage: http://chinageology.cgs.cn
https://www.sciencedirect.com/journal/china-geology

Application of tensor CSAMT with high-power orthogonal signal sources in Jiama porphyry copper deposit in Tibet

Peng-liang Yu[a], Ting Qu[a], Ri-zheng He[b,*], Jian-li Liu[a], Su-fen Wang[b], Xiao-long Chen[a]

[a] *Shaanxi Geology and Mining Geophysical and Geoehemical Prospecting Team Co., Tld., Xi'an* 710043, *China*
[b] *Chinese Academy of Geological Sciences*, *Beijing* 100037, *China*

ARTICLE INFO

Article history:
Received 13 April 2021
Received in revised form 6 January 0020
Accepted 15 July 2021
Available online 17 November 2021

Keywords:
Jiama porphyry copper deposit
Copper polymetallic deposit
Ultra-large-scale
Tensor CSAMT of 150 kw High power
2D inversion
Deep prospecting
Xizang (Tibet)

ABSTRACT

The Jiama porphyry copper deposit in Tibet is one of the proven ultra-large-scale copper deposits in the Qinghai-Tibet Plateau at present, with the reserves of geological resources equivalent to nearly 20×10^6 t. However, it features wavy and steep terrain, leading to extremely difficult field operation and heavy interference. This study attempts to determine the effects of the tensor controlled-source audio-magnetotellurics (CSAMT) with high-power orthogonal signal sources (also referred to as the high-power tensor CSAMT) when it is applied to the deep geophysical exploration in plateaus with complex terrain and mining areas with strong interference. The test results show that the high current provided by the high-power tensor CSAMT not only greatly improved the signal-to-noise ratio but also guaranteed that effective signals were received in the case of a long transmitter-receiver distance. Meanwhile, the tensor data better described the anisotropy of deep geologic bodies. In addition, the tests also show that when the transmitting current reaches 60 A, it is still guaranteed that strong enough signals can be received in the case of the transmitter-receiver distance of about 25 km, sounding curves show no near field effect, and effective exploration depth can reach 3 km. The 2D inversion results are roughly consistent with drilling results, indicating that the high-power tensor CSAMT can be used to achieve nearly actual characteristics of underground electrical structures. Therefore, this method has great potential for application in deep geophysical exploration in plateaus and mining areas with complex terrain and strong interference, respectively. This study not only serves as important guidance on the prospecting in the Qinghai-Tibet Plateau but also can be used as positive references for deep mineral exploration in other areas.

1. Introduction

The Jiama polymetallic deposit (Fig. 1) is located in the eastern section of the Gangdese metallogenic belt. It is a skarn-hornstone-porphyry copper polymetallic deposit closely related to Cenozoic intermediate-acid magmatic activities (Song L et al., 2011). Multiple generations of geological researchers have conducted extensive geological surveys with great efforts in Jiama area since the start of the 1950s, obtaining fruitful achievements. Jiama porphyry copper deposit ranks 91st in the world,the total resource amount is 6.296×10^6 t, with an average grade of 0.43%. It is determined that the Jiama copper polymetallic deposit boasts huge cumulative measured, indicated, inferred, and predicted intrinsically economic resources, in addition to copper, there are 1.37×10^6 t of lead, 4.723×10^5 t of zinc, 1.446×10^5 t of molybdenum, 100 t of gold, and 6.977×10^3 t of silver as of mid-2013.

The Jiama copper polymetallic deposit lies in Maizhokunggar County, Tibet Autonomous Region, covering an area of up to 144 km^2. It has an elevation of about 4780 m on average, with a minimum and maximum of nearly 4000 m and 5360 m, respectively. Therefore, it is a high-elevation deposit, with the oxygen content in the atmosphere being merely 40%−60% of that in plains and featuring an extreme climate perennially. Furthermore, it lies in the upper reach of the Lhasa River and shows a high-east and low-west terrain, leading to frequent natural disasters. Owing to the complex geological and terrain conditions and ongoing industrial mining (roadways and open blasting) in the Jiama ore

First author: *E-mail address*: 348632117@qq.com (Peng-liang Yu).

* Corresponding author: *E-mail address*: herizheng@cags.ac.cn (Ri-zheng He).

doi:10.31035/cg2021065
2096-5192/© 2021 China Geology Editorial Office.

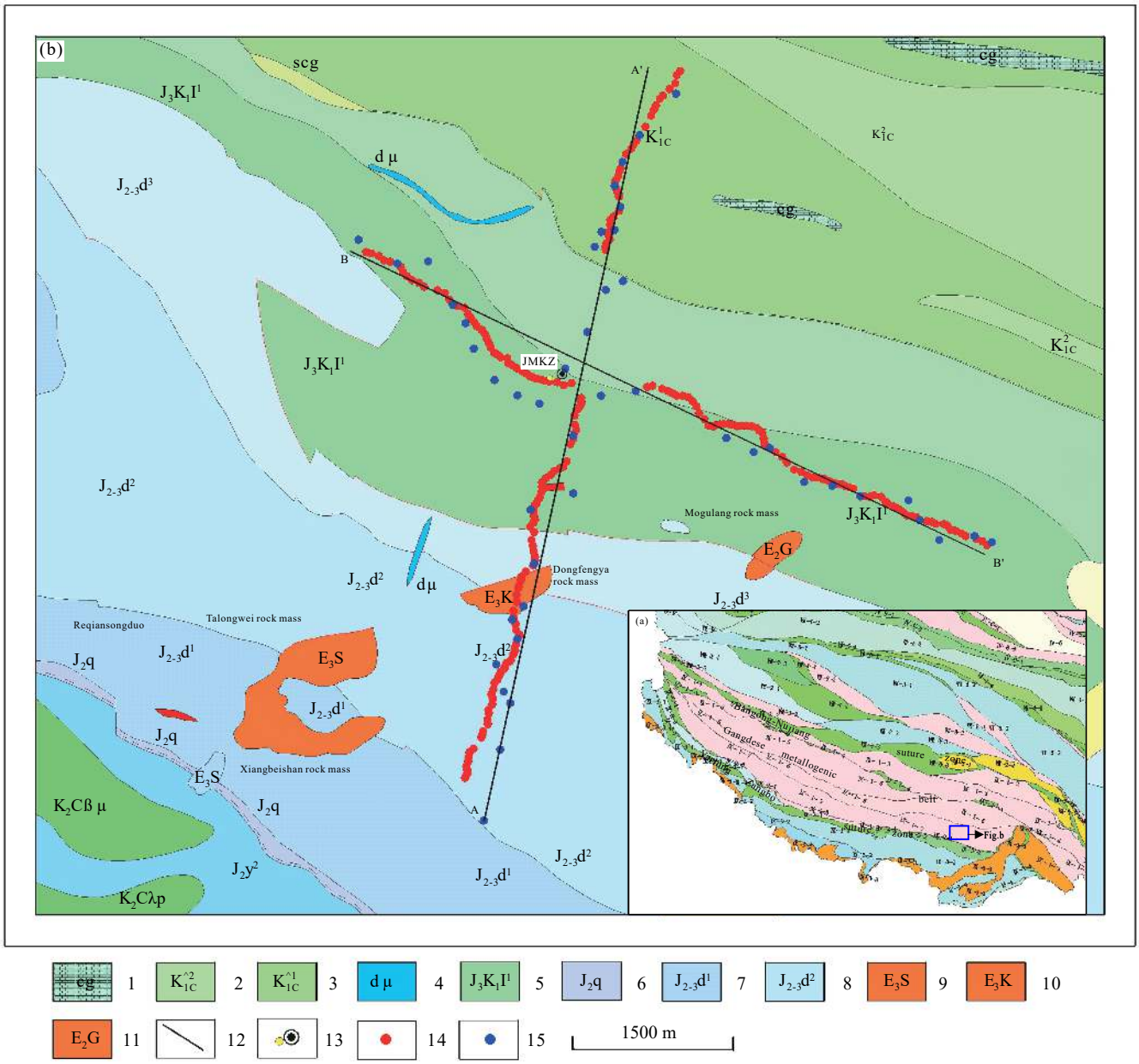

Fig. 1. Geologic map of the Jiama copper polymetallic deposit and the location of research section. (a)−geotectonic outline map of Tibet; (b)−geologic map of the Jiama copper polymetallic deposit (1:50000). 1−Glutenite; 2−Upper Member of Chumulong Formation; 3−Lower Member of Chumulong Formation; 4−Diorite porphyrite dike; 5−Linbuzong Formation; 6−Quesangwenquan Formation; 7−Lower Member of Duodigou Formation; 8−Upper Member of Duodigou Formation; 9−Biotite-hornblende tonalite in Shagelang Unit; 10−Adamellite porphyry in Kagazhai Unit; 11−Biotite monzogranite in Guoqinglang Unit; 12−Research section; 13−Location of scientific borehole JMKZ with a depth of 3000 m; 14−CSAMT measurement point; 15−MT measurement point.

concentration area, it is difficult to acquire the exploration data with a high signal-to-noise ratio in existing natural-source geophysical exploration (e.g., AMT and MT) in this area. This heavily impedes the breakthroughs in geophysical technologies for deep prospecting. This study aims to apply the high-power tensor CSAMT to prospecting research based on actual conditions in the Jiama ore concentration area and to summarize relevant technical processes for the further promotion and application of this method. This study not only serves as important guidance on the prospecting in the Qinghai-Tibet Plateau but also can be used as positive references for deep mineral exploration in other areas.

2. Geological background of Jiama copper polymetallic deposit

The Jiama copper polymetallic deposit lies in the front of the tectonic system of the NWW-trending Jiama-Kajunguo nappe (Zhong KH et al., 2012; Ma SW et al., 2016). The folds in the deposit exhibit NWW-trending axial traces. Among them, the Xiagongpu synclinorium and Niumatang anticlinorium are the secondary folds in the north wing of the Hong-Ta anticline. They are the ore-controlling structures of skarn deposits (Leng QF et al., 2015; Tang JX et al., 2013). The Tongshan gliding nappe has developed in the north wing

of the Hong-Ta anticline. It glides from south to north and its western part controls multiple skarn ore bodies. The outcrops in the Jiama copper polymetallic deposit include the Chumulong Formation (K_1c), Linbuzong Formation (J_3K_1l), and Duodigou Formation ($J_{2\text{-}3}d$) from south to north. Among them, the Upper Jurassic Duodigou Formation ($J_{2\text{-}3}d$) is composed of grayish-white marble and crystalline limestones, interbedded with marl, grayish-black calcirudites, and micritic calcirudites. The Lower Cretaceous Linbuzong Formation (J_3K_1l) can be divided into two parts. The upper part of it consists of lithic sandstones, quartz sandstones, and interbeds composed of lithic quartz siltstones and carbonaceous slates, while the lower part includes carbonaceous slates and carbonaceous shales interbedded with siltstones (Fig. 1). The intrusions in the Jiama copper polymetallic deposit were all formed during the Himalayan period (Ying LJ et al., 2006; Yu HQ et al., 2011). They are mainly distributed across the deposit and the areas to the north and east of the deposit. They include both type-I and type-S granites, both of which are calc-alkaline granites. In terms of rock types, they mainly include granite porphyry, granodiorite porphyry, and quartz albitophyres, as well as monzogranites, aplites, and diorite porphyrites. The intrusions mainly occur in the forms of batholiths, stocks, and dikes. A complete deposit model has been built for the Jiama ore concentration area based on the data obtained from exploration and extensive drilling (Tang JX et al., 2010). The ore bodies in the Jiama copper polymetallic deposit mainly include the following types. (1) Deep concealed porphyry molybdenum (copper) ore bodies. They are mainly controlled by the folds in the deposit and occur in a barrel shape in the middle part of the deposit. (2) Skarn copper polymetallic ore bodies. They occur surrounding the interlayer tectonic zones between the sand slates and hornstones in the Lower Cretaceous Linbuzong Formation and between the limestones and marbles in the Upper Jurassic Duodigou Formation. They are mainly under the control of the internal and external contact zones of rock masses and the expanded interlayer space resulting from nappe structures. They occur in laminated and stratoid forms in interlayer tectonic zones. (3) Copper-molybdenum (gold-sliver) ore bodies. They occur in the fissures and joint system of the hornstones on deep porphyries, showing a barrel shape. (4) Independent gold ore bodies occurring in peripheral tectonic fracture zones and diorite porphyrites. They are mainly controlled by the tensile faults at the periphery of rock masses. Among these four types of ore bodies, the laminated skarn copper polymetallic ones contain more than 70% of industrial ore reserves in the Jiama copper polymetallic deposit and thus are the most important.

3. Introduction of tensor CSAMT with high-power orthogonal signal sources

Based on the different skin effect produced during the propagation of natural-source planar electromagnetic waves after their vertical incidence into the ground, the natural-source magnetotelluric (MT) method was proposed by Tikhonov—a scientist from the former Soviet Union—and French scientist Garnier in the 1950s. It was not until the 1990s that the CSAMT began to gradually develop and be applied in China (He JS, 1990). Currently, CSAMT has widely been applied in mineral, groundwater, oil & gas, and engineering exploration, achieving significant effects (Tang JT and He JS, 2005). There are several types of CSAMT data measurement, namely scalar, vector, and tensor measurement. Li XB and Pedersen LB. (1991) gave the classic definition of the tensor CSAMT in sounding the earliest and deduced the impedance tensor and tipper of tensor CSAMT. Afterward, Deng QH (1993) translated relevant foreign work for the first time and conducted preliminary research. Boerner DE et al. (1993) firstly applied tensor CSAMT in the Cheynes deposit. In 2011, a German company, Metronix, successfully developed the first practical CSAMT electromagnetic (EM) instrument and its data processing software system for impedance tensor observation (Bernhard et al., 1993). The experts and researchers in China have conducted in-depth researches on the tensor CSAMT technology since 2013 (Meng QK et al., 2015, 2017; Lei D et al., 2014; Huang GY et al., 2014; Zhang ZY et al., 2017; Hu YC et al., 2015; Liu ZX et al., 2017; Zhou YD, 2015; Wang XX et al., 2014; Wang YM et al., 2018; Meng QK et al., 2013), achieving substantial test and research results as well as preliminary application(Di Q et al., 2020; Guo Z et al., 2019; Kouadio KL et al., 2020; Liu G et al., 2020). Although CSAMT possesses the advantages such as high efficiency and strong signals from an excited source of electromagnetic field, it has notable shortcomings. For instance, significant effects can be achieved when CSAMT is applied to the horizontal, uniform, and layered geological conditions (Di QY et al., 2008), but it is constrained by the power of the artificially excited source of electromagnetic field (also referred to as the artificial source), the geological conditions of the ground surface between the transmitters and receivers, and the near field effect of artificial sources (Wang G et al., 2008). Furthermore, it is heavily affected by objective conditions such as the financial cost of practical application. Given these, this paper introduces the practical case of applying high-power tensor CSAMT in the Jiama copper polymetallic deposit under complex geological conditions. As demonstrated by the preliminary results obtained, high-power tensor CSAMT can be widely applied.

Conventional scalar CSAMT is a two-component measurement consisting of an electric field component and a magnetic field component (E_x and H_y or E_y and H_x) excited by a single source. It commonly employs the equatorial array, and its effective measurement range consists of two sectors with an angle of 30° along the perpendicular bisector of two transmitting electrodes within the transmitter-receiver distance of $r \geq 4\delta$. In contrast, the high-power tensor CSAMT utilizes two separate or overlapped sources to measure 10 EM field components of the two sources (E_{x1}, E_{x2}, E_{y1}, E_{y2}, H_{x1}, H_{x2}, H_{y1}, H_{y2}, H_{z1}, and H_{z2}; Fig. 2). It is suitable for the

exploration of underground geologic bodies with complex geological or anisotropic characteristics, and its effective measurement range consists of eight sectors with an angle of 25°. In this manner, the high-power tensor CSAMT can be used to determine impedance tensor elements in four or even 6−10 directions compared with conventional CSAMT. Therefore, it is more suitable for obtaining accurate characteristics of 2D and 3D electrical structures under complex geological conditions.

4. Parameter selection and solution of data acquisition

4.1. Tests of transmitter-receiver distance

To choose a suitable transmitter-receiver distance, this study conducted tests of four different transmitter-receiver distances, namely 12 km, 17 km, 22 km, and 27 km, and the results are as follows (Fig. 3). When the transmitter-receiver distance was set at 12 km, smooth and continuous curves were obtained, but the near field occurred too early (at a frequency of about 10 Hz). As a result, it is difficult to realize the target exploration depth of 3 km. When the transmitter-receiver distance was 17 km, the resistivity curve obtained was not in the same order of magnitude as the resistivity curves obtained in the case of the other three transmitter-receiver distances. According to field investigation, the possible reason is that the underground geological structures and lithological features in this case are different from those in the other three cases, resulting in incomparable results. When the transmitter-receiver distance was set at 22 km and 27 km, continuous and smooth curves were obtained and they were slightly affected by the near field effect. Meanwhile, the target depth of 3 km was reached. Therefore, it is determined that the transmitter-receiver distance should be 22−27 km for the tensor CSAMT applied in the Jiama copper polymetallic deposit.

4.2. Tests of transmitting currents

Generally speaking, the higher the transmitting current, the stronger the signals. However, owing to the limitations of the power of transmitters (the maximum power is 150 kW and it suffers a loss in high-elevation areas) and economic benefit,

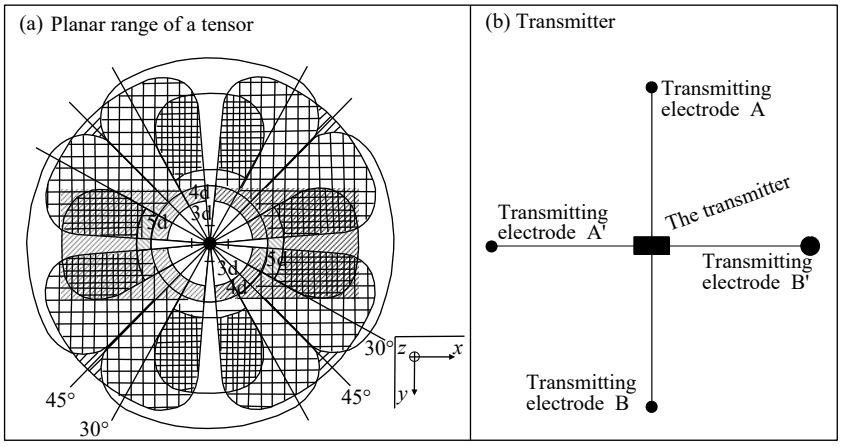

Fig. 2. Diagram of measurement range and observation means of tensor CSAMT. (a)-Planar range of a tensor; (b)-Transimitter

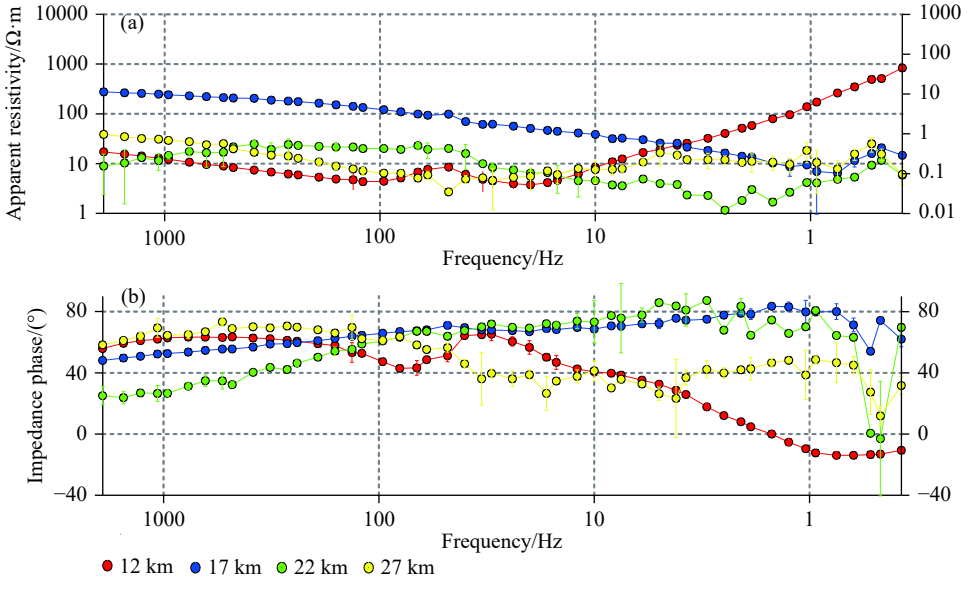

Fig. 3. Comparison of test curves in the case of different transmitter-receiver distances. (a)–resistivity curves; (b)–Phase curves.

the tests of small transmitting currents (20A, 40A) were also conducted to determine their effects. In detail, this study conducted the tests of transmitting currents of 20 A, 40 A, and 60 A under the constant voltage of 1500 V. As shown by the results (Fig. 4), the higher the transmitting current, the higher the data quality of the Jiama copper polymetallic deposit. Specifically, the curves with the highest quality were obtained in the case of the transmitting current of 60 A, while the curves are not ideal enough in the other two cases. Therefore, it is determined that the transmitting current should still be 60 A for the tensor CSAMT applied in the Jiama copper polymetallic deposit.

4.3. Tests of MN electrode spacing

The tests of MN electrode spacing were also conducted, in which the MN electrode spacing was set at 20 m, 50 m, and 75 m individually while other devices and parameters were fixed. The test results show (Fig. 5) that the larger the MN electrode spacing, the higher the quality of the Cagniard resistivity curves and impedance phase curves. However, owing to the greatly wavy terrain in the Jima copper polymetallic deposit and corresponding difficult field operation, large MN electrode spacing cannot be realized at many measurement points. Furthermore, relatively favorable effects can also be achieved when the MN electrode spacing was set at 50 m. Therefore, the MN electrode spacing was determined to be 50 m for the high-power tensor CSAMT in the Jima copper polymetallic deposit. Meanwhile, it was duly shortened (not less than 25 m) at the measurement points where it is extremely difficult to deploy electrodes.

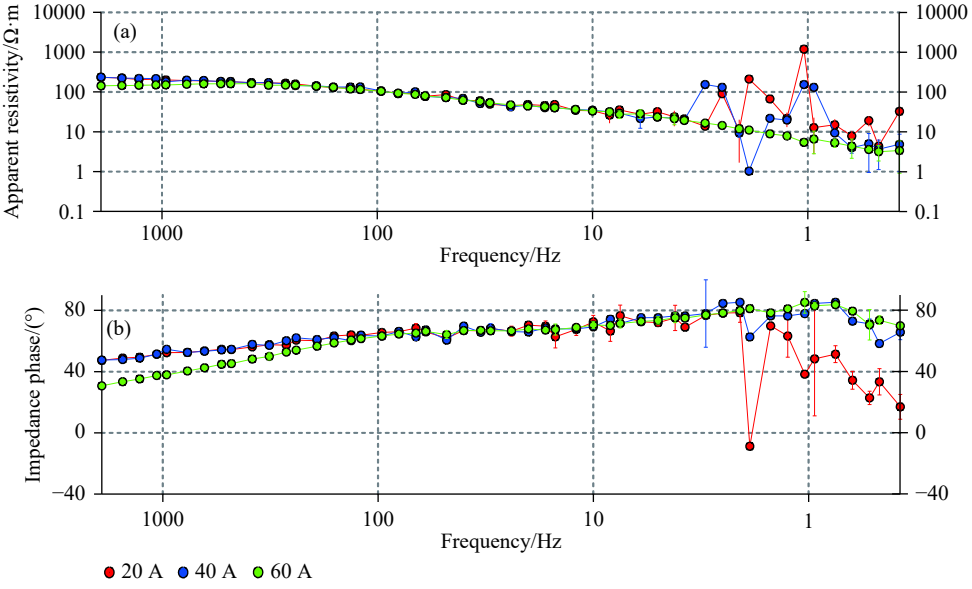

Fig. 4. Comparison of test curves in the case of different emission currents. (a)–resistivity curve; (b)–Phase curve.

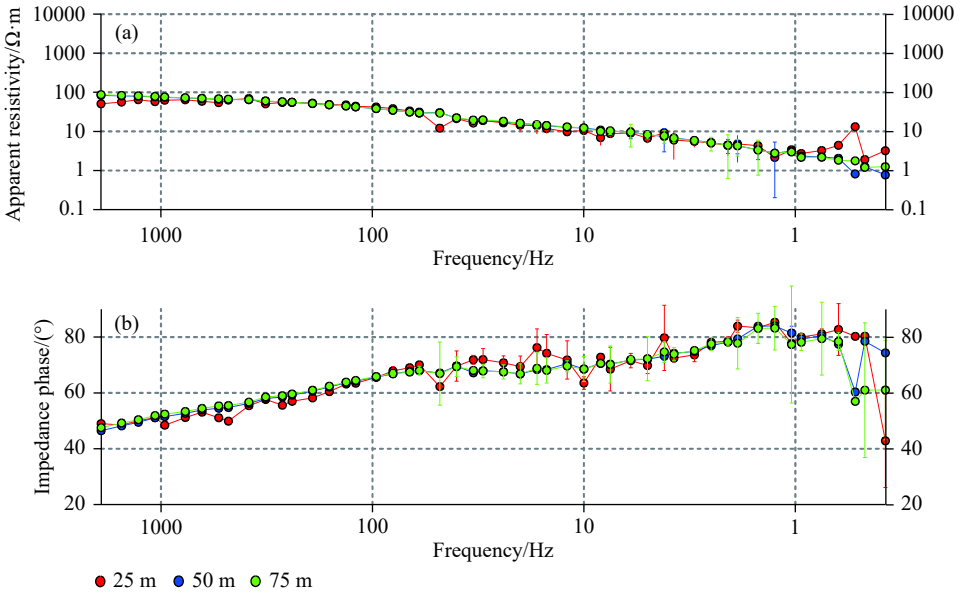

Fig. 5. Comparison of test curves in the case of different MN electrode spacing. (a)–resistivity curves; (b)–phase curves.

4.4. Tests of observation duration

It is necessary to select the most economical observation duration during field operation, besides selecting measurement points with flat terrain and small interference. Therefore, different observation duration (50 min, 60 min, and 70 min) was selected for test under the condition of the same source and same frequency. As indicated by the test results (Fig. 6), relatively high-quality Cagniard resistivity curves and impedance phase curves were obtained when the observation duration was set at 60 min or above. Based on this, the observation duration of the measurement points was determined to be 60 min for the tensor CSAMT applied in the Jima copper polymetallic deposit.

4.5. Main technical parameters

Based on the above tests, the technical parameters of the tensor CSAMT applied in the Jima copper polymetallic deposit were determined as follows. The transmitting and receiving instruments utilized in this study include the 150 kW transmitter SuperTX-150 and the multi-function V8 receiver with a frequency range of 0.375−1920 Hz produced by Canadian company Phoenix Geophysical. Two mutually perpendicular and overlapped field sources were employed, showing a cross shape. The AB electrodes were set at a distance of 3 km and an elevation of 3800−3900 m, with a maximum elevation difference of 131 m. The survey lines were set at an elevation of 4600−5300 m. The connecting wires between the transmitter and four electrodes have roughly the same length (Fig. 7). In terms of receiving ends, tensor observation was adopted. That is, five EM field components were measured, namely Ex, Ey, Hx, Hy, and Hz. Meanwhile, each V8 receiver controls two 3ERs. The main operating parameters were set as follows: AB electrode spacing: 3 km, resistivity of AB electrodes: 13 Ω and 16 Ω, respectively, transmitter-receiver distance: 23−27 km, transmitting current: 60−65 A, MN electrode spacing: 25−50 m, and observation duration: 1 h.

5. Electrical properties of rocks in the Jiama copper polymetallic deposit

To ensure the credibility and accuracy of data processing and interpretation, a systematical measurement was specifically conducted on the physical properties of cores from the Jiama ore concentration area (Qu T et al., 2021).

The electrical properties of the core specimens were measured using a SCIP tester manufactured by Instrumentation GDD Inc. of German, which operated in the microcurrent mode with a current output of 5 uA. The specimens were continuously powered for 8−16 s and then measured after 160 ms of time delay followed by power off. The core specimens were specially prepared. They were regular half-cylindrical or cylindrical in shape, with a length of 20−150 mm, and were immersed in water for more than 20 hours before being measured. Based on the resistivity data measured, the common scopes and modes of resistivity were calculated using the histogram method. As a result, the modes of resistivity of the hornstone, silicified hornstone, and skarn are about 2700 Ω·m, 2450 Ω·m, and 900 Ω·m, respectively; the average resistivity of the adamellite porphyry is 3542 Ω·m, and the modes of resistivity of the quartz diorite porphyrite, granodiorite porphyry, carbonaceous slate, and limestone are about 3900 Ω·m, 7500 Ω·m, 225 Ω·m, and 5000 Ω·m, respectively (Table 1, Fig. 8). As indicated by the measured data above, the hornstone, carbonaceous slate, skarn, intermediate-acidic intrusive rock, and limestone are of medium resistivity, low resistivity, medium-low resistivity, medium-high resistivity, and high resistivity, respectively.

6. Results from section inversion

Four sets of data were obtained at each measurement point

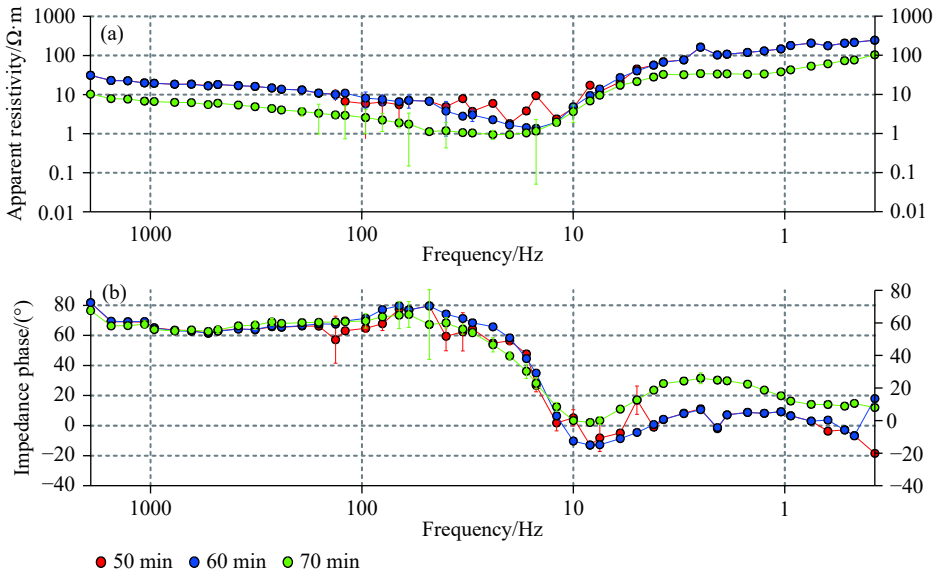

Fig. 6. Comparison of test curves in the case of different observation duration. (a)–resistivity curves; (b)–phase curves.

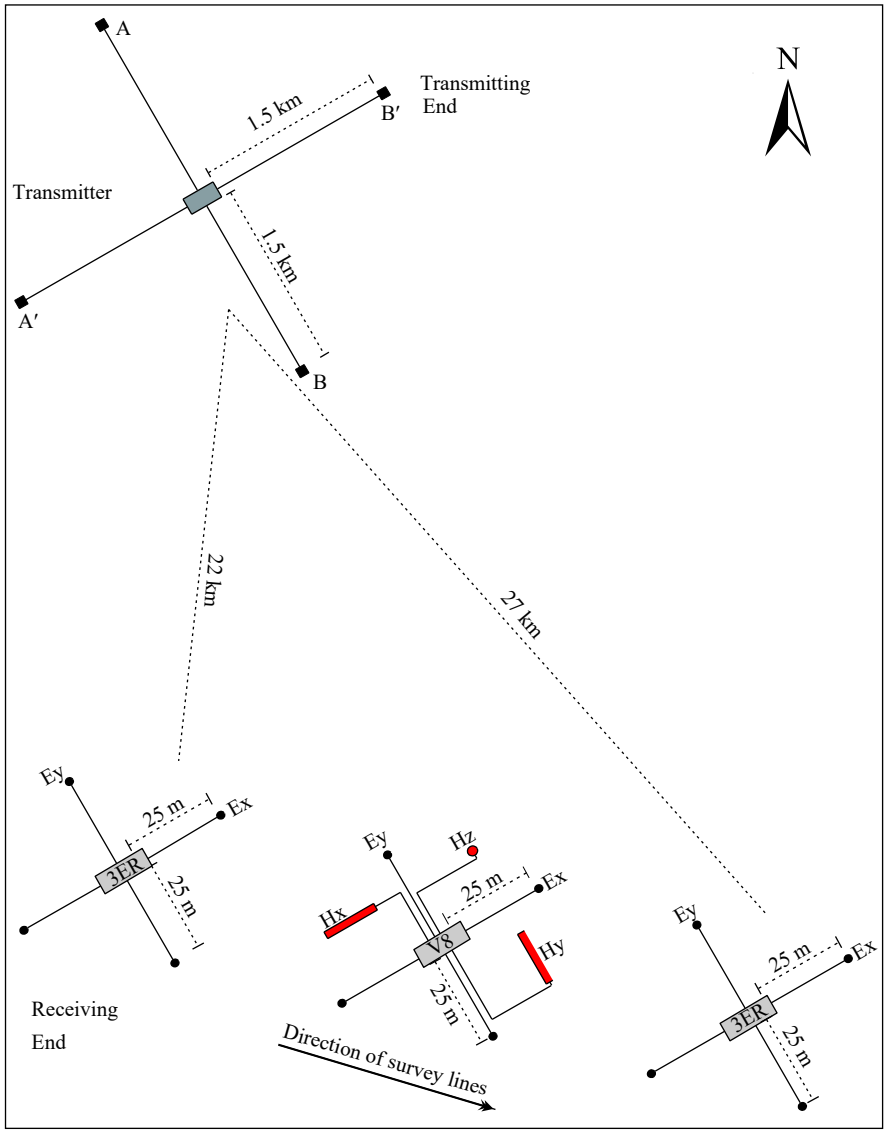

Fig. 7. Diagram of source and receiving devices of the high-power tensor CSAMT applied in the Jima copper polymetallic deposit.

Table 1. Statistics of resistivity of main rocks in the Jima copper polymetallic deposit.

Lithology	Number measured	Resistivity/Ω·m	
		Common range	Mode
Carbonaceous slate	27	150−400	225
Hornstone	216	1−7000	2700
Silicified hornstone	28	1−5600	2450
Skarn	25	1−2400	1400
Limestone	27	2000−8000	5000
Adamellite porphyry	12	2000−4000	3542
Quartz diorite porphyrite	36	2200−9900	3900
Granodiorite porphyry	48	5000−12000	7500

in the high-power tensor CSAMT, namely the data collected in the cases of EW-direction transmitting and NS-direction receiving, EW-direction transmitting and EW-direction receiving, NS-direction transmitting and NS-direction receiving, and NS-direction transmitting and EW-direction receiving (Fig. 9). The data curves collected in different transmitting and receiving directions slightly differ in terms of morphology. However, notably high-quality data were generally obtained when the receiving ends were in the direction of the perpendicular bisector of AB electrodes (transmitting ends).

2D inversion of four sets of CSAMT data along section BB ’ was conducted using scalar CSAMT inversion technology, during which program MTPioneer was employed. Prior to the 2D inversion, interpolation in the frequency domain was conducted for all measurement points along section BB ’. As a result, 50 effective frequencies were obtained, with a frequency range of 1920−0.375 Hz. In terms of the parameters used for inversion, the transverse magnetic (TM) mode was adopted in a unified way, with the threshold error and initial regularization factor set at 5% and 200, respectively. The inversion ended after 41 iterations and the root-mean-square (RMS) errors of four models of electrical properties varied in the range of 8.5−10.3. Finally, four types of inversion results were obtained (Fig. 10), from which it can be seen that the stratum structures reflected by the four sets of

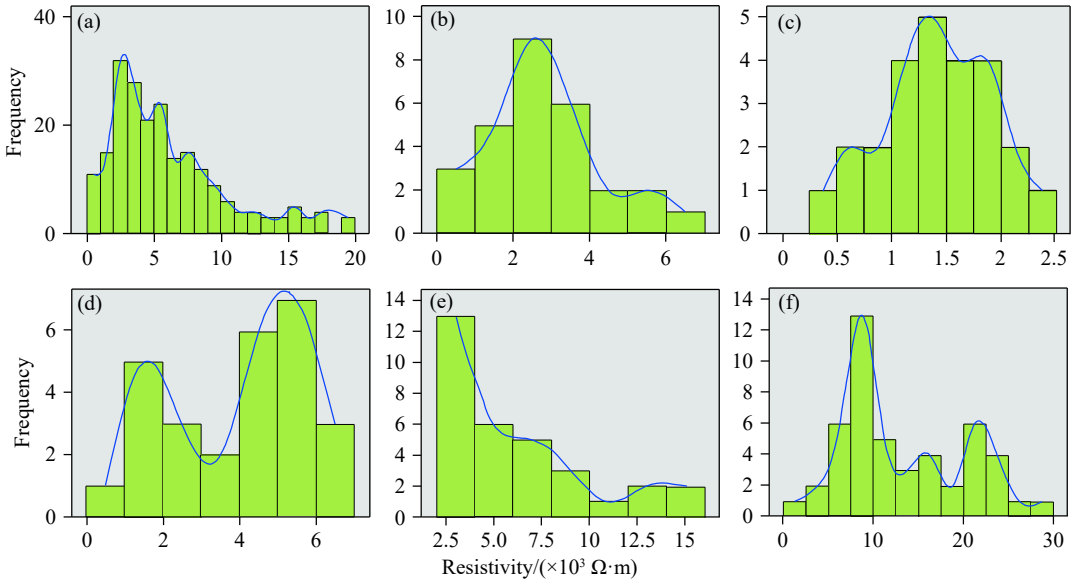

Fig. 8. Histograms for resistivity measurement of main rocks in the Jima copper polymetallic deposit. (a)–Hornstone; (b)–Silicified hornstone; (c)–Skarn; (d)–Limestone; (e)–Quartz diorite porphyrite; (f)–Granodiorite porphyry.

data are highly similar overall but are slightly different in some details. For instance, high-resistivity bodies are reflected in the deep parts of both the western and eastern segments of section BB ’. However, their extension toward deep parts differs to some extent, which may represent different lithological characteristics (Table 1, Fig. 8). Furthermore, high-resistivity bodies at a depth of about 2−2.5 km are reflected by all the four types of inversion results. However, they are somewhat different in morphology. Overall, the shallow low-resistivity and near-surface high-resistivity bodies reflected are roughly consistent, as shown in Fig. 10.

Fig. 11 shows the apparent resistivity pseudosections obtained from the 2D inversion of sections AA’ and BB’. In the CSAMT and MT measurement, the distance between measurement points is 50 m and 250 m, respectively, the survey lines roughly coincide, and the inversion depth is 3 km and 5 km, respectively. Meanwhile, the TM mode was adopted for the inversion of sections AA’ and BB’. The 2D CSAMT inversion results of section AA’ (Fig. 11a) are as follows. The southern segment of the apparent resistivity pseudosection shows medium-high resistivity overall, which is interpreted as the limestones of the Duodigou Formation based on the electrical properties and outcrops (Fig. 1). The top of the northern segment of the pseudosection shows laminated low-resistivity bodies. Based on this as well as the corresponding outcrops of the quartz sandstones in the Chumulong Formation, the laminated low-resistivity bodies are interpreted as the quartz sandstones of the Chumulong Formation. The lower part of the northern segment of the pseudosection shows medium-low resistivity. Meanwhile, the local outcrops corresponding to this part are the hornstones of the Linbuzong Formation. Therefore, the medium-low resistivity is interpreted as the hornstones of the Linbuzong Formation. There are blocky high-resistivity bodies in local areas of the pseudosection, which are interpreted as intermediate-acidic intrusions based on the characteristics of the electrical properties.

The 2D inversion results of the MT and CSAMT data along section AA ’ (Fig. 11a, b) show similar electrical structures. In detail, the northern segment mainly reflects medium-low-resistivity hornstones of the Linbuzong Formation, the southern segment mainly represents the medium-high-resistivity limestones of the Duodigou Formation, and the deep cloudy high-resistivity anomalies reflect intermediate-acidic intrusions. However, the shallow electrical structures reflected by the 2D MT inversion results (Fig. 11b) suffer notably lower resolution and precision than those reflected by the 2D CSAMT inversion results (Fig. 11a). The 2D CSAMT inversion results of section BB’ (Fig. 11c) show that the electrical structures along the section consist of two layers in general. Among them, the upper layer exhibits medium-low resistivity overall and the outcrops include the hornstones of the Linbuzong Formation. Meanwhile, the lower layer shows medium-high resistivity overall, which is interpreted as the hornstones of the Duodigou Formation based on the electrical properties. Besides, there are high-resistivity anomalies locally, which are interpreted as intermediate-acidic intrusions based on the electrical properties. The 2D MT and CSAMT inversion results (Figs. 11d, c) of section BB ’ are roughly the same. However, the former show notably poorer details of the shallow part than the latter. The distinct reasons include much sparser measurement points in the MT measurement compared to the CSAMT measurement (Fig. 1) and the strong resistance to noise of the high-power controlled sources (Fig. 7) stated in this paper.

On the whole, existing exploration model shows that the strata in the Jiama copper polymetallic deposit consist of the quartz sandstones of the Chumulong Formation, the slates of the Linbuzong Formation, the hornstones of the Linbuzong

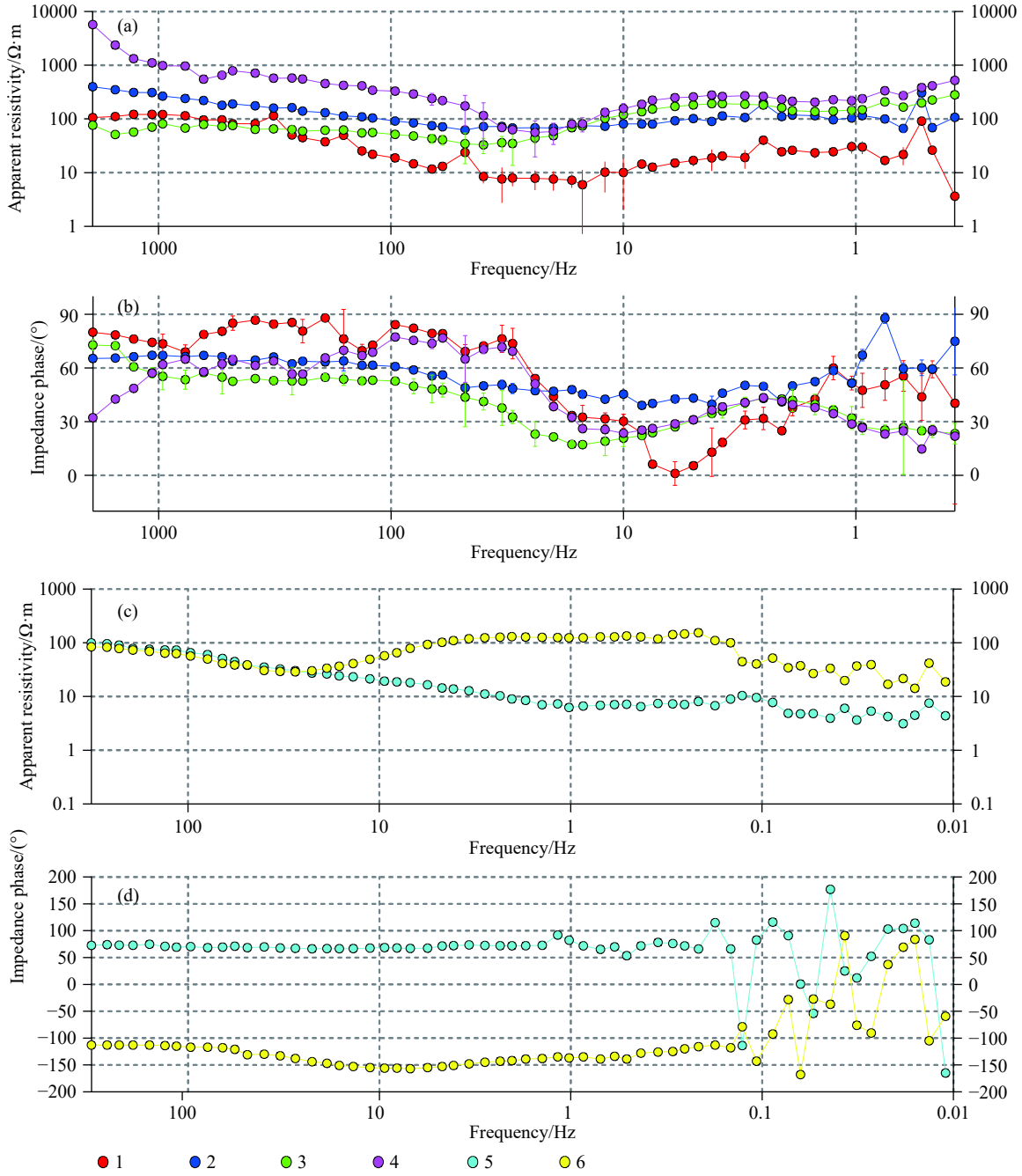

Fig. 9. Comparison of CSAMT curves collected in the case of different transmitting and receiving directions. (a)–CSAMT resistivity curves collected in the case of different transmitting and receiving directions; (b)–CSAMT phase curves collected in the case of different transmitting and receiving directions; (c)–MT resistivity curves; (d)–MT phase curves. 1–CSAMT curve collected in the case of EW-direction transmitting and NS-direction receiving; 2–CSAMT curve collected in the case of EW-direction transmitting and EW-direction receiving; 3–CSAMT curve collected in the case of NS-direction transmitting and NS-direction receiving; 4–CSAMT curve collected in the case of NS-direction transmitting and EW-direction receiving; 5–MT curve collected in the case of xy direction; 4. MT curve collected in the case of yx direction.

Formation, and the limestones of the Duodigou Formation from top to bottom. Meanwhile, these strata incline toward the north overall, resulting in a north-inclined nappe structure (Tang JX et al., 2011). Among them, the quartz sandstones of the Chumulong Formation and the slates of the Linbuzong Formation are distributed in limited areas. As shown in Fig. 10 and 11, skarn is mainly distributed in the contact zones between the Duodigou and Linbuzong formations. Besides, the intermediate-acidic intrusions intruding into the Duodigou and Linbuzong formations provided rich metallogenic substances (Fig. 11b, d).

7. Verification of drilling data

As shown in Fig. 1, borehole JMKZ is roughly located in section BB' and is about 150 m away from section AA'. It can be divided into three parts in terms of its composition. The part at a depth of less than 600 m primarily consists of hornstones, with laminated quartz diorite porphyrites

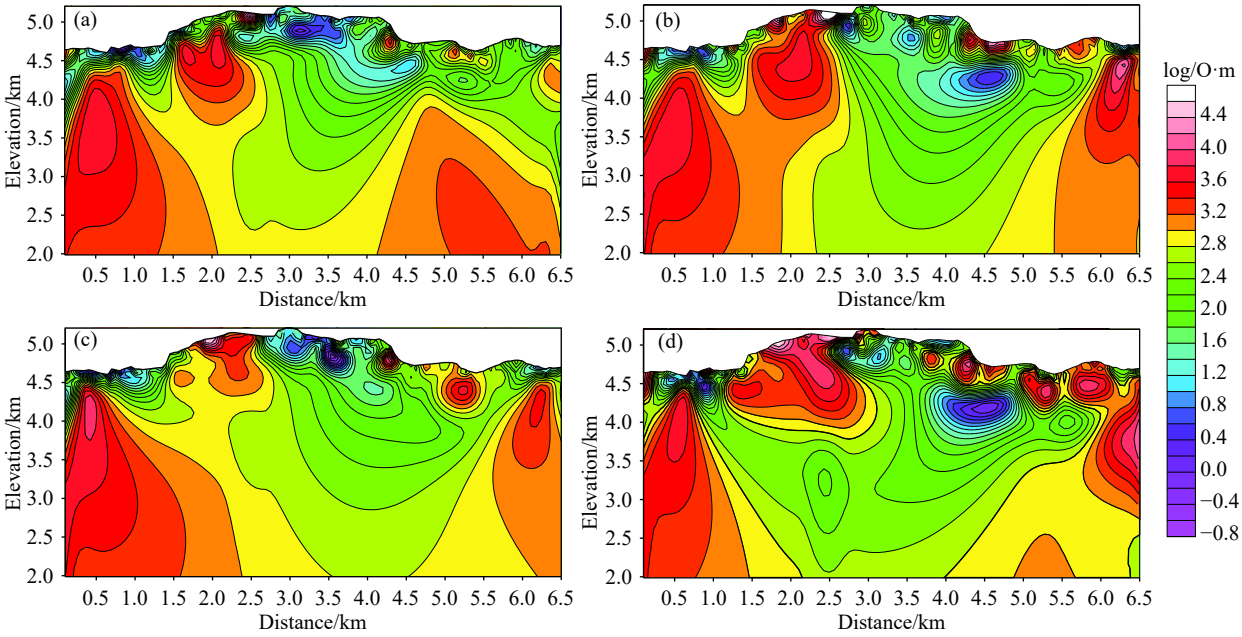

Fig. 10. 2D inversion results of four sets of high-power tensor CSAMT data along section BB'. (a)–EW-direction transmitting and NS-direction receiving; (b)–EW-direction transmitting and EW-direction receiving; (c)–NS-direction transmitting and NS-direction receiving; (d)–NS-direction transmitting and EW-direction receiving.

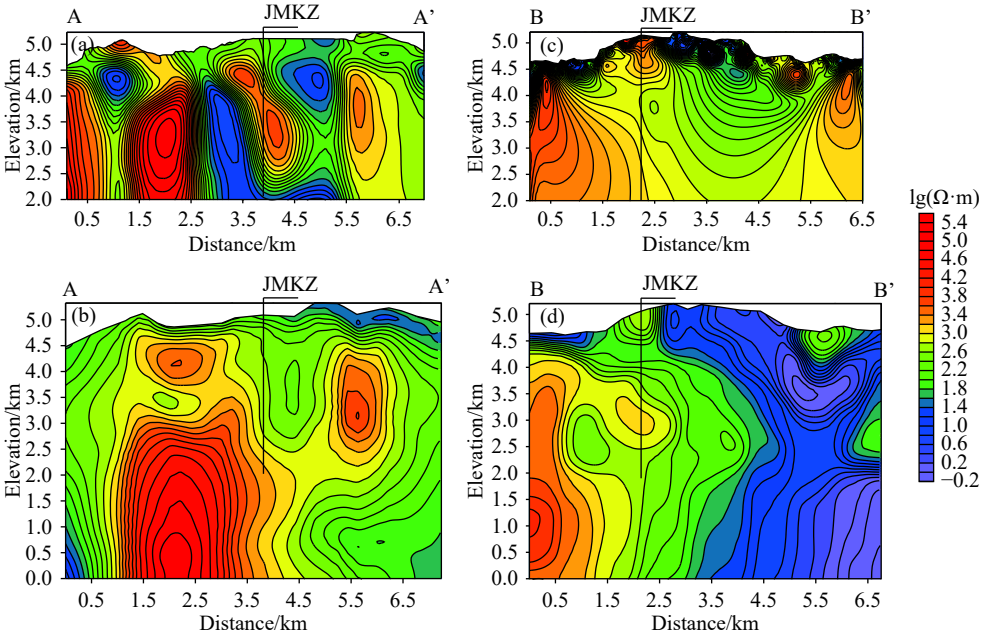

Fig. 11. Comparison of 2D inversion results of tensor CSAMT and MT data of sections AA' and BB'. (a)–2D CSAMT inversion results of section AA'; (b)–2D MT inversion results of section AA'; (c)–2D CSAMT inversion results of section BB'; (d)–2D MT inversion results of section BB'; JMKZ is a scientific borehole with a depth of 3000 m (see Fig. 1 for its location).Vertical variation of resistivity along JMKZ borehole see Fig. 12.

distributed locally. The part at a depth of 600−900 m is mainly composed of skarn and serves as the major hosting strata of skarn-type ore bodies. Meanwhile, the part at a depth of greater than 900 m mainly includes intrusive rock masses.

In this study, the core specimens from scientific borehole JMKZ were measured using a SCIP tester manufactured by Instrumentation GDD Inc. of German. The sampling interval was set at 10 m and 300 core specimens were measured (Fig. 12). Fig. 12 shows the resistivity and polarizability curves (Figs. 12a, b). The core specimens mainly exhibit four types of physical properties, and the details are as follows. (1) The part at a depth of less than 600 m mainly shows low resistivity and low polarization, with local quartz diorite porphyrites exhibiting high resistivity and low polarization. (2) The part at a depth of 600−900 m mainly features low resistivity and high polarization. Therefore, this part is similar to the overall

physical structure of the ore bodies in the Jiama ore concentration area. (3) The part at a depth of 900−2100 m is characterized by high resistivity and sawtooth-shaped polarizability, which is possibly induced by local veined mineralization of the intrusive rock masses in this part. (4) The part at a depth of greater than 2100 m is characterized by low resistivity and low polarization.

The electrical properties at the location of borehole JMKZ reflected by 1D CSAMT inversion results of section AA' are basically the same as measurement results of the core specimens. According to the 1D CSAMT inversion results of section AA', the apparent resistivity varies in a low-high-low trend and the part at a depth of 600−2100 m especially shows marked low-high-low change of apparent resistivity (Fig. 12c). Meanwhile, the 1D MT inversion results show that the apparent resistivity varies from low to high (Fig. 12d). All these comprehensively indicate that the high-power tensor CSAMT adopted in the study is practical and reliable. The electrical properties at the location of borehole JMKZ reflected by 1D CSAMT and MT inversion results of section BB' are slightly different from the measurement results of the core specimens. Both the CSAMT and MT inversion results reflect the presence of shallow high-resistivity bodies. This is possibly induced by the anomalies of quartz diorite

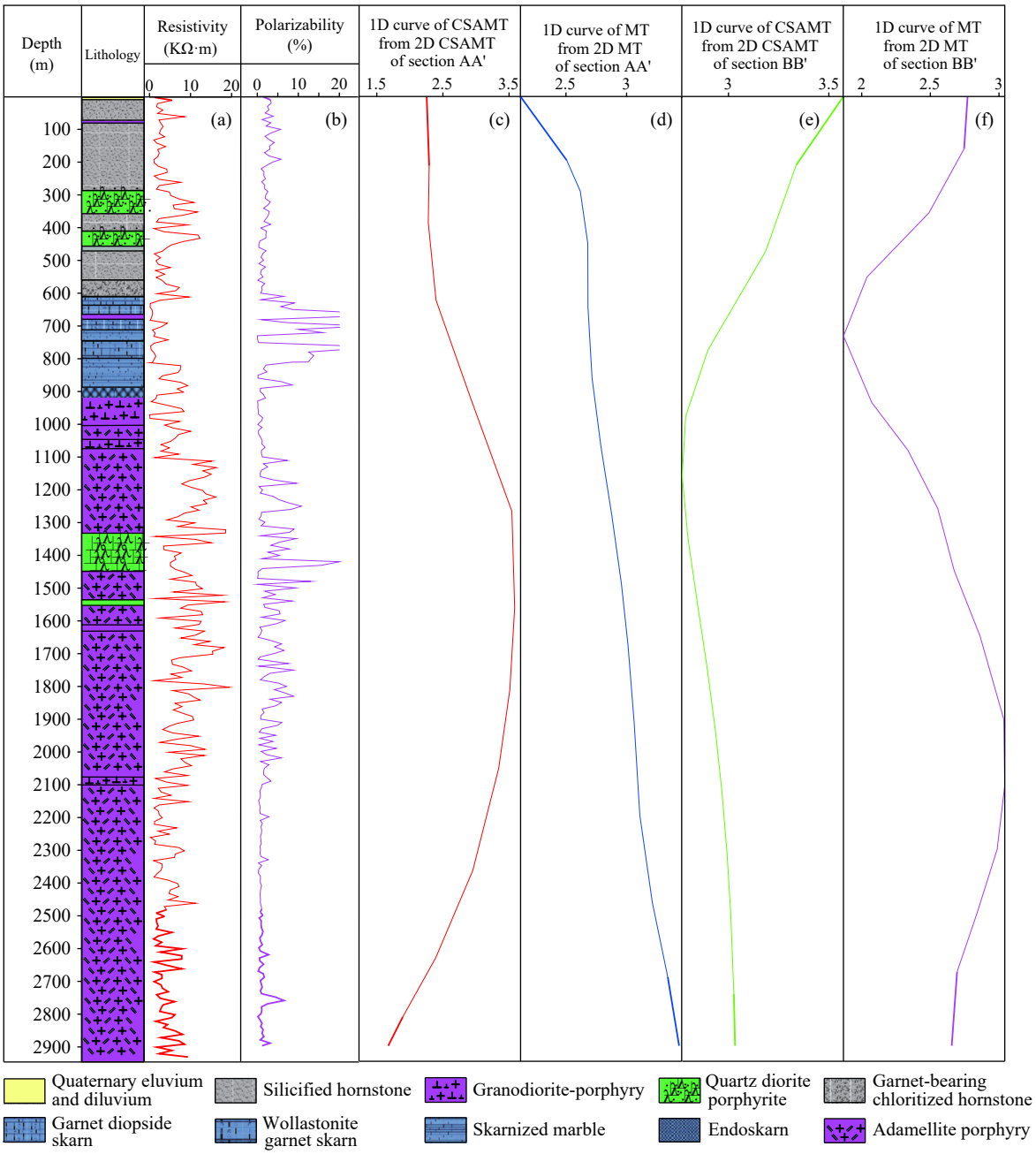

Fig. 12. Histogram and curves obtained from core specimen measurement of JMKZ borehole, and inverted resistivity variation across JMKZ from MT and CSAMT of sections AA' and BB' in Fig. 11. (a)– measured resistivity in JMKZ Borehole; (b)– measured polarizability in JMKZ Borehole; (c)– inverted 1D CSAMT curve of section AA'; (d)– inverted 1D MT curve of section AA'; (e)– inverted 1D CSAMT curve of section BB'; (f)– inverted 1D MT curve of section BB'. Those location for (c), (d), (e), and (f) see successively (a), (b), (c) and (d) in Fig. 11.

porphyrites, which are similar to the measurement results of the core specimens that the shallow quartz diorite porphyrites show high resistivity (Fig. 12a). Most especially, the horizon with low apparent resistivity reflected by the MT inversion results is roughly consistent with the lithological and electrical structure anomalies of JMKZ (Fig. 12a). Therefore, the changes in the deep electrical properties reflected by the inversion results of this study are generally credible.

To sum up, the structures obtained from the 1D inversion of both high-power tensor CSAMT data (Figs. 11a, c) and natural-source MT data (Figs. 11b, d) are consistent with the structure determined by the physical-property measurement results of the core specimens from scientific borehole JMKZ (Figs. 12a, b). Meanwhile, they are also in agreement with the overall characteristics of physical structure in the Jiama ore concentration area. The consistent structural characteristics obtained by different means indicated that the high-power tensor CSAMT can be used to achieve an exploration depth of 3 km, data with a high signal-to-noise ratio (Fig. 9, Fig. 11), and nearly actual characteristics of underground electrical structures. There, significant effects can be achieved when the high-power tensor CSAMT is applied in the deep prospecting in mining areas.

8. Conclusions

This study explored the effects of the high-power tensor CSAMT when it is applied in the Jima copper polymetallic deposit with complex plateau terrain and strong interference. As a result, it was verified that significant effects can be achieved when the high-power tensor CSAMT is applied to the deep geophysical exploration in mining areas.

As indicated by the results of this study, the high current provided by the high-power tensor CSAMT improved the signal-to-noise ratio and ensured that effective signals can be received in the case of a long transmitter-receiver distance. Meanwhile, the anisotropy of deep geological bodies can be well described by the tensor data. In addition, tests in this study show that when the transmitting current reached 60 A, it is still guaranteed that strong enough signals can be received in the case of the transmitter-receiver distance of about 25 km, the sounding curves show no near field effect, and effective exploration depth can reach 3 km. The 2D inversion results are roughly consistent with drilling results, indicating that high-power tensor CSAMT can be used to achieve nearly actual characteristics of underground electrical structures. Therefore, this method has great potential for application in deep geophysical exploration in plateaus with complex terrain and mining areas with strong interference.

Although high-quality tensor CSAMT data were acquired in this study, it should be noted that 3D inversion results that can further reflect the advantages of tensor exploration data (Fig. 9) are yet to be obtained due to the current immature inversion technology of tensor CSAMT data. This is also the direction of future research.

CRediT authorship contribution statement

Peng-liang Yu and Ting Qu completed the study of section inversion and comparative analysis. Ri-zheng He conceived and planned the study and oversaw its implementation and compiled all of figures. Jian-li Liu gave theoretical guidance and verification to the research results. Su-fen Wang and Xiao-long Chen completed the parameter test and physical property statistics. Peng-liang Yu wrote the manuscript with the support of Ri-zheng He, Ting Qu, Jian-li Liu, Su-fen Wang and Xiao-long Chen. All authors discussed the results and contributed to the final manuscript.

Declaration of competing interest

The authors declare no conflict of interest.

Acknowledgment

The authors would like to extend their sincere gratitude to Professor Ju-xing Tang and Dr. Pan Tang from the Institute of Mineral Resources, Chinese Academy of Geological Sciences, Professor Deng-hai Bai from the Institute of Geology and Geophysics, Chinese Academy of Science, Professor Jing-tian Tang from the Central South University, and Professor Jian-en Jing from the China University of Geosciences for their guidance and assistance during field data collection and indoor data processing in this study. This work was together supported by the National Key Research and Development Program of China (2018YFC0604102), and the Geological Investigation Project (DD20190015). Owing to the limitation on the authors' knowledge and paper length, this paper only introduced the actual application of the high-power tensor CSAMT in the Jima copper polymetallic deposit. The authors will appreciate any comments and corrections to any omissions and errors.

References

Boerner DE, Wright JA, Thurlow JG, Reed LE. 1993. Tensor CSAMT studies at the Buchans mine in central Newfoundland. Geophysics, 58(1), 12–19. doi: 10.1016/0148-9062(93)92442-S.

Bernhard F. 2011. Multi dipole CSAMT. The 10th China International Geo-Electromagnetic Workshop. Nanchang, Chinese Geophysical Society, 96−99.

Deng QH, Li XB, Pedersen LB. 1993. Magnetotelluric method with controllable source tensor. Translation of Seismogeology, 15(3), 35–42 (in Chinese with English abstract).

Di QY, Wang R. 2008. Forward and Inverse Modeling of Controlled Source Audio Magnetotelluric Data and Its Application. Beijing, Science Press, 98−115.

Di Q, Fu C, An Z, Wang R, Wang G, Wang M, Qi S, Liang P. 2020. An application of CSAMT for detecting weak geological structures near the deeply buried long tunnel of the Shijiazhuang-Taiyuan passenger railway line in the Taihang Mountains. Engineering Geology, 268(1), 105517. doi: 10.1016/j.enggeo.2020.105517.

Gui B. 2015. Two-dimensional inversion of tensor data from controlled-source audio-frequency magnetotelluric method. Master's Dissertation, China University of Geosciences (Beijing) (in Chinese with English abstract).

Guo Z, Hu L, Liu C, Cao C, Liu R. 2019. Application of the CSAMT Method to Pb –Zn Mineral Deposits: A Case Study in Jianshui. Minerals, 9(12), 726. doi: 10.3390/min9120726.

He JS. 1990. Controlled Source Audio Frequency Magnetotelluric Method. Changsha, Central South University of Technology Press, 25−37 (in Chinese).

Huang GY, Zhang GH. 2014. Comparative test of tensor and scalar measurements in known iron ore areas. Geophysical and Geochemical Exploration, 38(6), 1207–1211 (in Chinese with English abstract). doi: 10.11720/wtyht.2014.6.21.

Hu YC, Li TL, Fang CS. 2015. 3D tensor CSAMT forward modeling based on vector finite element method. Applied Geophysics, 12(1), 35–46. doi: 10.1007/s11770-014-0469-1.

Huang GY, Zhang GH. 2017. Application of impedance rotation in two dimensional inversion of tensor CSAMT. Journal of Engineering Geophysics, 14(1), 13–19 (in Chinese with English abstract). doi: 10.3969/j.issn.1672-7940.2017.01.003.

Kouadio KL, Xu Y, Liu CM, Zakaria B. 2020. Two-dimensional inversion of CSAMT data and three-dimensional geological mapping for groundwater exploration in Tongkeng Area. Journal of Applied Geophysics, 183. doi: 10.1016/j.jappgeo.2020.104204.

Lei D, Zhang GH, Huang GY. 2014. Application of tensor controlled source audio magnetotelluric method. Journal of Engineering Geophysics, 11(3), 286–294 (in Chinese with English abstract). doi: 10.3969/j.issn.1672-7940.2014.03.003.

Li XB, Pedersen LB. 1991. Controlled-source tensor magnetotelluric. Geophysics, 56(9), 1456–1461. doi: 10.1190/1.1443165.

Leng FQ, Tang JX, Zheng WB. 2015. Study on ore-controlling factors of thick and large skarn orebody in Jiama porphyry metallogenic system in Tibet. Ore Deposit Geology, 34(2), 273–288 (in Chinese with English abstract). doi: 10.16111/j.0258-7106.2015.02.005.

Liu ZX, Xue GQ, Zhang LB. 2017. Comparative analysis of tensor CSAMT effective observation area simulation. Acta Geophysica Sinica, 60(8), 3278–3287 (in Chinese with English abstract).

Liu G, Meng X, Tan H, Chen Z, Liu L. 2020. Case study: joint seismic reflection and CSAMT data interpretation for mineral explorations in Fujian. Acta Geophysica, 68(5), 1–13. doi: 10.1007/s11600-020-00477-2.

Meng QK. 2013. Preliminary study on data acquisition and processing technology of tensor CSAMT. Master's Dissertation, Chinese Academy of Geological Sciences (in Chinese with English abstract).

Meng QK, Ling PR, Xu BL. 2013. One dimensional numerical simulation of tensor CSAMT. Calculation Technology of Geophysical and Geochemical exploration, 35(4), 435–441 (in Chinese with English abstract). doi: 10.3969/j.issn.1001-1749.2013.04.11.

Meng QK, Lin PR, Li Y, Li JH, Zhu HW, Li D. 2015. Preliminary study and demonstration of tensor CSAMT data processing technology. Journal of Jilin University (Earth Science Edition), 46(6), 1846–1854 (in Chinese with English abstract). doi: 10.13278/j.cnki.jjuese.201506302.

Ma SW, Xu ZQ, Zhang ZK. 2016. Tectonic deformation and its restriction on mineralization of Jiama copper-polymetallic deposit in southern Tibet. Acta Petrologica Sinica, 32(12), 3781–3799 (in Chinese with English abstract).

Qu T, He RZ, Yu PL. 2021. Statistics and application of rock physical properties in Jiama mining area, Tibet. Geophysical and Geochemical Exploration, 45(3), 661–668 (in Chinese with English abstract). doi: 10.11720/wtyht.2021.1014.

Song L, Wang XW, Tang JX. 2011. From jet genesis to porphyry-skarn metallogenic system, some implications for successful exploration of Jiama copper polymetallic deposit. Ore Deposit Geology, 30(2), 219–230 (in Chinese with English abstract). doi: 10.16111/j.0258-7106.2011.02.005.

Tang JT, He JS. 2005. Controlled Source Audio Frequency Magnetotelluric Method and its Application. Changsha, Central South University Press, 57−66 (in Chinese).

Tang JX, Wang DH, Wang XW. 2010. Geological characteristics and deposit model of Jiama copper polymetallic deposit in Tibet. Acta Geoscientica, 31(4), 495–506 (in Chinese with English abstract). doi: 10.3975/cagsb.2010.04.02.

Tang JX, Deng SL, Zheng WB. 2011. Exploration model of Jiama copper polymetallic deposit in Mozhugongka County, Tibet. Ore Deposit Geology, 30(2), 179−196 (in Chinese with English abstract). 179−196. doi: 10.16111/j.0258–7106.2011.02.002.

Tang JX, Zheng WB, Chen YC. 2013. Exploration breakthrough of deep porphyry orebody in Jiama copper-polymetallic deposit, Tibet and its significance. Journal of Jilin University (Earth Science Edition), 43(4), 1100–1110 (in Chinese with English abstract). doi: 10.13278/j.cnki.jjuese.2013.04.018.

Wang G, Wang SM, Lei D. 2011. Experimental study on CSAMT field source effect. Calculation Technology of Geophysical and Geochemical Exploration, 33(5), 527–530 (in Chinese with English abstract). doi: 10.3969/j.issn.1001-1749.2011.05.012.

Wang XX, Di QY, Xu C. 2014. Multi dipole source characteristics and tensor measurement of CSAMT. Acta Geophysica Sinica, 57(2), 651–661 (in Chinese with English abstract).

Wang G, Zhang ZY, Li YB. 2016. Tensor controlled source audio magnetotelluric method and its application. Computing Techniques for Geophysical and Geochemical Exploration, 5, 37–44 (in Chinese with English abstract). doi: 10.3969/j.issn.1001-1749.2016.05.04.

Wang YM, Zhang GH, You M. 2018. Simulating the field source effect of tensor CSAMT method with forward modeling method. Geophysical and Geochemical Exploration Calculation Technology, 40(1), 82–88 (in Chinese with English abstract). doi: 10.3969/j.issn.1001-1749.2018.01.12.

Yu HQ, Feng CY, Zhang DQ. 2006. Comparative study on fluid inclusion characteristics of Jama skarn type copper polymetallic deposit and Qulong porphyry type copper deposit in Gangdisi copper belt, Tibet. Acta Petrologica Sinica, 22(3), 689–696 (in Chinese with English abstract). doi: 10.3969/j.issn.1000-0569.2006.03.018.

Ying LJ, Tang JX, Wang DH. 2011. Mineralization age of porphyry dikes and its relationship with mineralization in Jiama super-large copper deposit, Tibet. Acta Petrologica Sinica, 27(7), 2095–2102 (in Chinese with English abstract).

Zhong HK, Li L, Zhou HW. 2012. Characteristics of the Nappe tectonic system in Jiama-Kajunguo, Tibet. Acta Geoscientia Sinica, 33(4), 411–423 (in Chinese with English abstract). doi: 10.3975/cagsb.2012.04.03.

Zhou YD. 2015. Characteristics and tensor measurement of CSAMT multi dipole sources. Master's Dissertation, Chengdu University of Technology (in Chinese with English abstract).

Zhang YS. 2016. Tensor CSAMT two-dimensional forward inversion of undulating terrain. Master's Dissertation, China University of Geosciences (Beijing), 35−42 (in Chinese with English abstract). doi: CNKI:CDMD:2.1016.184578.

Zhang ZY, Wang G, Hu XY. 2017. Tensor CSAMT method and comparative experiment. Petroleum Geophysical Exploration, 52(4), 869–874 (in Chinese with English abstract). doi: 10.13810/j.cnki.issn.1000-7210.2017.04.025.